dominant and recessive Cx26 mutations in pedigrees with non-syndromic deafness. In addition, Cx26 expression was demonstrated in human cochlear cells. Therefore, combined mutation and expression data implicate Cx26 as the gene responsible for deafness in these and possibly other families linked to 13q11–12 (DFNA3 and DFNB1), making it the first non-syndromic sensorineural deafness gene to be discovered. A role for gap junctions in the recycling of potassium ions back to the endolymph of the cochlear duct after stimulation of the sensory hair cells has been suggested[18], and the loss of Cx26 would be expected to disrupt this potassium ion flow, leading to the loss of hearing. A feature of the individuals homozygous for Cx26 truncations was the lack of any other observable phenotype, even though Cx26 is widely expressed in other tissues, for example, the liver and the pancreas[11]. It is unclear how the M34T mutation leads to the dominant-negative phenotype, or if functional channels can form and how these might interact with wild-type channels. This is the third human disease in which connexin mutations have been reported, the others being Cx32 in X-linked Charcot-Marie-Tooth disease (which may also be associated with deafness)[21] and Cx43 in visceroatrial heterotaxia syndrome[22]. The identification of connexin mutations in these and other human diseases will aid our understanding of their biology. □

Methods

Haplotype and linkage analysis. Lymphocyte DNA extracted from family members was genotyped by PCR amplification of microsatellite marker loci mapping to 13q11–12 with fluorescently labelled primers. Primer sequences were obtained from the Genome Database. The PCR products were run on a 373A Automated DNA sequencer running Genescan software (Applied Biosystems). Alleles were analysed using Genotyper software (Applied Biosystems). Linkage analysis has been described[19].

Screening of Cx26 gene for mutations. The coding exon was amplified using PCR and specific primers that produced two overlapping PCR products. The four primer sequences used were: 5′-TCTTTTCCAGAGCAAACCGC-3′ with 5′-GACACGAAGATCAGCTGCAG-3′ and 5′-GGGCAATGCGTTAAACTGGC-3′ with 5′-CCAGGCTGCAAGAACGTGTG-3′. The Cx26 sequence was taken from GenEmbl accession number M86849. PCR conditions were 35 cycles of denaturation at 95 °C for 1 min, annealing at 60 °C for 1 min, and extension at 72 °C for 30 s. PCR products were band-purified on a 1% low-melting-point agarose gel using Wizard spin purification columns (Promega). The products were sequenced directly from both ends using an AmpliTaq Cycle sequencing kit and ABI Prism 377 DNA sequencer.

Immunohistochemical analysis. Skin biopsy material was obtained from the non-dominant hypothenar eminence, abdomen and psoriatic plaques from volunteers and snap-frozen in liquid nitrogen. Human cochlea was obtained post mortem from a 76-year-old woman 36 h after death. The cochlea was identified by serial microslicing of the temporal bone and was removed by microdissection. The cochlea was embedded in Cryo-M-Bed (Bright) and snap-frozen in liquid nitrogen. Immunochemical analysis was performed on serial 5-μm cryostat sections using a standard technique[17]. Every fifth section was stained with haemotoxylin and eosin to assess orientation. The polyclonal rabbit anti-connexin 26 antibody (Zymed) was used at a 1/100 dilution.

Received 14 January; accepted 20 March 1997.

1. Morton, N. E. Genetic epidemiology of hearing impairment. *Ann. N.Y. Acad. Sci.* **630,** 16–31 (1991).
2. Tassabehji, M. *et al.* Waardenburg's syndrome patients have mutations in the human homologue of the *Pax-3* paired box gene. *Nature* **355,** 635–636 (1992).
3. Tassabehji, M. *et al.* Mutations in the *PAX3* gene causing Waardenburg syndrome type 1 and type 2. *Nature Genet.* **3,** 26–30 (1993).
4. Weil, D. *et al.* Defective myosin VIIA gene responsible for Usher syndrome 1B. *Nature* **374,** 60–61 (1995).
5. Verbov, J. Palmoplantar keratoderma, deafness and atopy. *Br. J. Dermatol.* **116,** 881–882 (1987).
6. Fitzgerald, D. A. & Verbov, J. L. Hereditary palmoplantar keratoderma with deafness. *Br. J. Dermatol.* **134,** 939–942 (1996).
7. Guilford, P. *et al.* A human gene responsible for neurosensory, non-syndromic recessive deafness is a candidate homologue of the mouse *sh*-1 gene. *Hum. Mol. Genet.* **3,** 989–993 (1994).
8. Chaib, H. *et al.* A gene responsible for a dominant form of neurosensory non-syndromic deafness maps to NSRD1 recessive deafness gene interval. *Hum. Mol. Genet.* **3,** 2219–2222 (1994).
9. Kibar, Z. *et al.* The gene responsible for Clouston hidrotic ectodermal dysplasia maps to the pericentromeric region of chromosome 13q. *Hum. Mol. Genet.* **5,** 543–547 (1996).
10. Mignon, C. *et al.* Assignment of connexin 26 (GJB2) and 46 (GJA3) genes to human chromosome 13q11–q12. *Cytogenet. Cell Genet.* **72,** 185–186 (1996).
11. Kumar, N. M. & Gilula, N. B. The gap junction communication channel. *Cell* **84,** 381–388 (1996).
12. Beyer, E. C. Gap junction. *Int. Rev. Cytol.* **137,** 231–242 (1993).
13. Kumar, N. M. & Gilula, N. B. Molecular biology and genetics of gap junction channels. *Semin. Cell Biol.* **3,** 3–16 (1992).
14. Risek, B., Klier, F. G. & Gilula, N. B. Multiple gap junction genes are utilized during rat skin and hair development. *Development* **116,** 639–651 (1992).
15. Goliger, J. A. & Paul, D. L. Expression of gap junction proteins Cx26, Cx31.1, Cx37, and Cx43 in developing and mature epidermis. *Dev. Dyn.* **200,** 1–13 (1994).
16. Yeager, M. & Nicholson, B. J. Structure of gap junction intercellular channels. *Curr. Opin. Struct. Biol.* **6,** 183–192 (1996).
17. Markey, A. C., Lane, E. B., MacDonald, D. M. & Leigh, I. M. Keratin expression in basal cell carcinomas. *Br. J. Dermatol.* **126,** 154–160 (1992).
18. Kikuchu, T., Kimar, R. S., Paul, D. L. & Adams, J. C. Gap junctions in the rat cochlea: immunohistochemical and ultrastructural analysis. *Anat. Embryol.* **191,** 101–118 (1995).
19. Brown, K. A. *et al.* Linkage studies in non-syndromic recessive deafness (NSRD) in a family originating from the Mirpur region of Pakistan maps DFNB1 centromeric to D13S175. *Hum. Mol. Genet.* **5,** 169–173 (1996).
20. Petit, C. Genes responsible for human hereditary deafness: a symphony of a thousand. *Nature Genet.* **14,** 385–391 (1996).
21. Bergoffen, J. *et al.* Connexin mutations in X-linked Charcot-Marie-Tooth Disease. *Science* **262,** 2039–2041 (1993).
22. Britz-Cunningham, S. H., Shah, M. M., Zuppan, C. W. & Fletcher, W. H/ Mutations of the connexin-43 gap function gene in patients with heart malformations and defects of laterality. *N. Engl. J. Med.* **332,** 1323–1329 (1995).

Acknowledgements. We thank P. Spink and C. Chronnell for technical support; J. Verbov and R. E. Kelsell for DNA samples; D. J. Roberts, J. Verbov and H. Forsythe for audiograms; and J. Pitts, M. Finbow and I. A. McKay for discussion. This work was supported in part by grants from the Wellcome Trust (D.P.K., H.P.S., N.J.L., R.F.M. and I.M.I.), the MRC (J.D.) and the ICRF (H.P.S., I.M.L.).

Correspondence and requests for materials should be addressed to D.P.K. (e-mail: David_P_Kelsell @sbphrd.com.uk).

Regulation of skeletal muscle mass in mice by a new TGF-β superfamily member

Alexandra C. McPherron*, Ann M. Lawler† & Se-Jin Lee*

** Department of Molecular Biology and Genetics, and † Department of Gynecology and Obstetrics, Johns Hopkins University School of Medicine, 725 North Wolfe Street, Baltimore, Maryland 21205, USA*

The transforming growth factor-β (TGF-β) superfamily encompasses a large group of growth and differentiation factors playing important roles in regulating embryonic development and in maintaining tissue homeostasis in adult animals[1]. Using degenerate polymerase chain reaction, we have identified a new murine TGF-β family member, growth/differentiation factor-8 (GDF-8), which is expressed specifically in developing and adult skeletal muscle. During early stages of embryogenesis, GDF-8 expression is restricted to the myotome compartment of developing somites. At later stages and in adult animals, GDF-8 is expressed in many different muscles throughout the body. To determine the biological function of GDF-8, we disrupted the GDF-8 gene by gene targeting in mice. GDF-8 null animals are significantly larger than wild-type animals and show a large and widespread increase in skeletal muscle mass. Individual muscles of mutant animals weigh 2–3 times more than those of wild-type animals, and the increase in mass appears to result from a combination of muscle cell hyperplasia and hypertrophy. These results suggest that GDF-8 functions specifically as a negative regulator of skeletal muscle growth.

To identify new members of the TGF-β superfamily, we designed degenerate oligonucleotides corresponding to conserved regions among the known family members and used these oligonucleotides as primers for polymerase chain reaction (PCR) on mouse genomic DNA. Among the new sequences obtained in this screen was one that we designated GDF-8. A full-length GDF-8 complementary DNA clone obtained from screening a murine skeletal muscle library contained a single long open reading frame encoding a protein 376 amino acids long. The predicted GDF-8 amino-acid sequence contains all of the hallmarks characteristic of members of

the TGF-β superfamily, including a signal sequence for secretion, a proteolytic processing site, and a carboxy-terminal region containing the conserved pattern of cysteine residues (Fig. 1a). Like the TGF-βs and inhibin-βs, GDF-8 contains nine cysteine residues in the C-terminal region. However, on the basis of pairwise comparisons of the C-terminal region of GDF-8 with those of the other members of the TGF-β superfamily, GDF-8 does not appear to fall into any of the known subfamilies of highly related factors, including the TGF-βs, inhibins and bone morphogenetic proteins (BMPs) (Fig. 1b). In the C-terminal region, GDF-8 is most homologous to Vgr-1 (45% amino-acid identity).

Like most other TGF-β family members, GDF-8 also appears to be highly conserved across species. By genomic Southern analysis, homologous sequences were detected in all mammalian species examined as well as in chickens (Fig. 1c). In most species, the GDF-8 probe also detected a second, more faintly hybridizing fragment. Further analysis of GDF-8-homologous sequences in murine and human DNA revealed that this second fragment corresponds to a highly related gene, GDF-11 (A.C.M. and S.-J.L., unpublished results); the isolation of GDF-11 and characterization of GDF-11 knock-out mice will be described elsewhere.

To determine whether the processing signals in the GDF-8 sequence are functional and whether GDF-8 forms dimers as do other members of the TGF-β superfamily, the GDF-8 cDNA was stably expressed in Chinese hamster ovary (CHO) cells. As shown in Fig. 1d, western analysis of conditioned medium prepared from these cells using an antiserum raised against a bacterially expressed C-terminal fragment of GDF-8 detected two protein species with apparent relative molecular masses (M_r) of about 52,000 (52K) and 15,000 (15K) under reducing conditions, consistent with unprocessed and processed forms of GDF-8, respectively. No bands were obtained either with preimmune serum or with conditioned medium from CHO cells transfected with an antisense construct (data not shown). Under non-reducing conditions, the GDF-8 antiserum detected two predominant protein species with apparent M_rs of about 101K and 25K, consistent with dimeric forms of unprocessed and processed GDF-8, respectively. Hence, like other TGF-β family members, GDF-8 appears to be secreted and proteolytically processed, and the C-terminal region appears to be capable of forming a disulphide-linked dimer.

To determine the expression pattern of GDF-8, *in situ* hybridization was performed on mouse embryos isolated at various stages of development. At all stages examined, the expression of GDF-8 messenger RNA appeared to be restricted to developing skeletal muscle. At early stages, GDF-8 expression was restricted to developing somites. By whole-mount *in situ* hybridization analysis, GDF-8 mRNA could first be detected as early as day 9.5 post-coitum (p.c.) in about one-third of the somites (Fig. 2a). At this stage of development, hybridization appeared to be restricted to the most mature (9 out of 21 in the example shown) rostral somites. By day 10.5 p.c. (Fig. 2b), GDF-8 expression was clearly evident in almost every somite (26 out of 33 in the example shown). On the basis of *in situ* hybridization analysis of sections prepared from day 10.5 p.c. embryos, the expression of GDF-8 in somites appeared to be localized to the myotome compartment (Fig. 2c). At later stages of development, GDF-8 expression was detected in a wide range of developing muscles. Examples of GDF-8 expression in developing muscles of the foot and hip region at day 14.5 p.c. are shown in Fig. 2d, e.

GDF-8 continues to be expressed in adult animals as well. By northern analysis, GDF-8 mRNA expression was seen almost exclusively in skeletal muscle among the different adult tissues examined (Fig. 2f). A significantly lower although clearly detectable signal was also seen in adipose tissue. On the basis of northern analysis of RNA prepared from a large number of different adult skeletal muscles, GDF-8 expression appeared to be widespread although the expression levels varied among individual muscles (Fig. 2g).

To determine the biological function of GDF-8, we disrupted the GDF-8 gene by homologous targeting in embryonic stem cells. To ensure that the resulting mice would be null for GDF-8 function, the entire mature C-terminal region was deleted and replaced by a neo cassette (Fig. 3a). Homologous targeting of the GDF-8 gene was seen in 13/131 gancyclovir/G418 doubly resistant embryonic stem (ES) cell clones. Following injection of these targeted clones into blastocysts, we obtained chimaeras from five independently derived ES clones that produced heterozygous pups when crossed to C57BL/6 females. Genotypic analysis (Fig. 3b) of 678 offspring derived from crosses of F1 heterozygotes showed 170+/+ (25%), 380+/− (56%) and 128 −/− (19%). Although the ratio of genotypes was close to the expected ratio of 1 : 2 : 1, the smaller than expected number of homozygous mutants appeared to be statistically significant

Table 1 Total body weights of homozygous, heterozygous and wild-type animals

Genotype	Weight (g)			
	2 months	3 months	4 months	5 months
		Male		
+/+	28.0 ± 3.0 (n = 18)	30.6 ± 3.7 (n = 35)	33.2 ± 4.4 (n = 26)	33.9 ± 3.9 (n = 20)
+/−	29.1 ± 2.9 (n = 53)	31.9 ± 4.0 (n = 90)	34.6 ± 3.9 (n = 68)	36.1 ± 3.3 (n = 59)
−/−	36.2 ± 4.0 (n = 23)*	41.0 ± 4.5 (n = 33)*	43.1 ± 3.5 (n = 23)*	42.9 ± 5.0 (n = 18)*
		Female		
+/+	22.1 ± 2.0 (n = 12)	23.7 ± 3.2 (n = 35)	26.1 ± 3.6 (n = 16)	27.2 ± 3.3 (n = 19)
+/−	23.1 ± 2.6 (n = 31)	26.0 ± 2.9 (n = 53)†	27.6 ± 3.3 (n = 36)	28.8 ± 3.6 (n = 35)
−/−	26.2 ± 2.3 (n = 10)*	30.8 ± 3.8 (n = 21)*	32.7 ± 3.9 (n = 12)*	35.1 ± 3.8 (n = 15)*

* Significant difference between +/+ and −/− ($P < 0.001$).
† Significant difference between +/+ and +/− ($P < 0.01$).

Table 2 Weights of individual muscles from mutant and wild-type animals

	Weight (g)*		Per cent of +/+
	+/+ (n = 9)	−/− (n = 9)	
Body	30.3 ± 3.3	40.9 ± 4.2	135
Digastric	0.022 ± 0.005	0.045 ± 0.007	205
Pectoralis	0.178 ± 0.042	0.467 ± 0.067	262
Triceps brachii	0.158 ± 0.036	0.372 ± 0.039	235
Quadriceps	0.232 ± 0.052	0.470 ± 0.053	203
Gastrocnemius/plantaris	0.150 ± 0.033	0.328 ± 0.020	219
Tibialis cranialis	0.047 ± 0.005	0.095 ± 0.017	202
Soleus	0.006 ± 0.002	0.012 ± 0.001	200

* Significant difference between +/+ and −/− with $P < 0.001$.

Table 3 Carcass analysis of homozygous, heterozygous and wild-type animals

Genotype	Weight (g)		
	Body	Carcass	Fat
+/+ (n = 4)	31.92 ± 3.63	22.84 ± 2.41	2.01 ± 0.46
+/− (n = 5)	32.76 ± 1.36	23.87 ± 1.12	2.17 ± 0.78
−/− (n = 5)	42.28 ± 2.67*	33.94 ± 2.07†	2.01 ± 0.30

Significant difference between +/+ and −/− with $P < 0.01$ (*) and $P < 0.001$ (†).

a

```
1   MMQKLQMYVY IYLFMLIAAG PVDLNEGSER EENVEKEGLC NACAWRQNTR   50
51  YSRIEAIKIQ ILSKLRLETA PNISKDAIRQ LLPRAPPLRE LIDQYDVQRD  100
101 DSSDGSLEDD DYHATTETII TMPTESDFLM QADGKPKCCF FKFSSKIQYN  150
151 KVVKAQLWIY LRPVKTPTTV FVQILRLIKP MKDGTRYTGI RSLKLDMSPG  200
201 TGIWQSIDVK TVLQNWLKQP ESNLGIEIKA LDENGHDLAV TFPGPGEDGL  250
251 NPFLEVKVTD TPKRSRRDFG LDCDEHSTES RCCRYPLTVD FEAFGWDWII  300
301 APKRYKANYC SGECEFVFLQ KYPHTHLVHQ ANPRGSAGPC CTPTKMSPIN  350
351 MLYFNGKEQI IYGKIPAMVV DRCGCS  376
```

b

	GDF-8	MIS	inhibin α	inhibin βA	inhibin βB	inhibin βC	GDF-10	BMP-3/osteogenin	BMP-2	BMP-4	BMP-5	Vgr-1(BMP-6)	OP-1(BMP-7)	OP-2(BMP-8)	GDF-5(CDMP-1)	GDF-6(CDMP-2)	GDF-7	GDF-1	GDF-3/Vgr-2	GDF-9	nodal	lefty	GDNF	TGF-ß1	TGF-ß2	TGF-ß3
GDF-8	100	31	26	38	42	38	36	38	41	38	42	45	42	40	37	38	37	35	41	27	33	22	16	34	37	37
MIS	-	100	18	24	25	29	31	30	27	27	24	24	27	27	27	26	25	34	22	21	22	15	18	28	23	25
inhibin α	-	-	100	26	25	26	29	29	22	22	24	25	24	26	24	25	26	23	25	26	23	25	20	23	22	24
inhibin βA	-	-	-	100	63	53	35	36	42	41	43	44	43	42	40	43	41	37	42	30	39	19	18	41	37	36
inhibin βB	-	-	-	-	100	54	34	37	42	42	37	41	42	37	37	38	36	35	41	30	37	25	22	35	34	37
inhibin βC	-	-	-	-	-	100	30	31	37	36	37	35	38	35	36	36	38	40	34	28	36	20	18	33	34	35
GDF-10	-	-	-	-	-	-	100	83	46	45	42	44	42	40	43	42	42	40	39	28	40	24	19	29	30	29
BMP-3/osteogenin	-	-	-	-	-	-	-	100	48	47	43	44	42	41	47	44	46	42	42	29	41	25	17	32	32	32
BMP-2	-	-	-	-	-	-	-	-	100	92	61	61	60	55	57	54	57	42	53	34	42	21	23	35	34	36
BMP-4	-	-	-	-	-	-	-	-	-	100	59	60	58	55	57	55	57	43	50	35	40	21	22	34	33	35
BMP-5	-	-	-	-	-	-	-	-	-	-	100	91	88	74	52	54	52	46	50	31	40	20	23	34	35	36
Vgr-1(BMP-6)	-	-	-	-	-	-	-	-	-	-	-	100	87	75	51	53	52	46	53	31	43	21	21	35	37	39
OP-1(BMP-7)	-	-	-	-	-	-	-	-	-	-	-	-	100	74	51	53	53	47	50	30	41	18	22	34	38	38
OP-2(BMP-8)	-	-	-	-	-	-	-	-	-	-	-	-	-	100	50	51	53	47	55	27	44	21	24	30	35	38
GDF-5(CDMP-1)	-	-	-	-	-	-	-	-	-	-	-	-	-	-	100	82	80	46	48	32	42	15	22	33	34	37
GDF-6(CDMP-2)	-	-	-	-	-	-	-	-	-	-	-	-	-	-	-	100	82	43	46	32	43	17	22	34	35	37
GDF-7	-	-	-	-	-	-	-	-	-	-	-	-	-	-	-	-	100	48	45	33	45	18	24	36	35	38
GDF-1	-	-	-	-	-	-	-	-	-	-	-	-	-	-	-	-	-	100	50	28	35	18	18	33	32	33
GDF-3/Vgr-2	-	-	-	-	-	-	-	-	-	-	-	-	-	-	-	-	-	-	100	32	40	19	24	36	31	32
GDF-9	-	-	-	-	-	-	-	-	-	-	-	-	-	-	-	-	-	-	-	100	31	19	20	22	25	24
nodal	-	-	-	-	-	-	-	-	-	-	-	-	-	-	-	-	-	-	-	-	100	18	19	28	32	31
lefty	-	-	-	-	-	-	-	-	-	-	-	-	-	-	-	-	-	-	-	-	-	100	12	25	23	27
GDNF	-	-	-	-	-	-	-	-	-	-	-	-	-	-	-	-	-	-	-	-	-	-	100	19	17	21
TGF-ß1	-	-	-	-	-	-	-	-	-	-	-	-	-	-	-	-	-	-	-	-	-	-	-	100	74	78
TGF-ß2	-	-	-	-	-	-	-	-	-	-	-	-	-	-	-	-	-	-	-	-	-	-	-	-	100	82
TGF-ß3	-	-	-	-	-	-	-	-	-	-	-	-	-	-	-	-	-	-	-	-	-	-	-	-	-	100

c

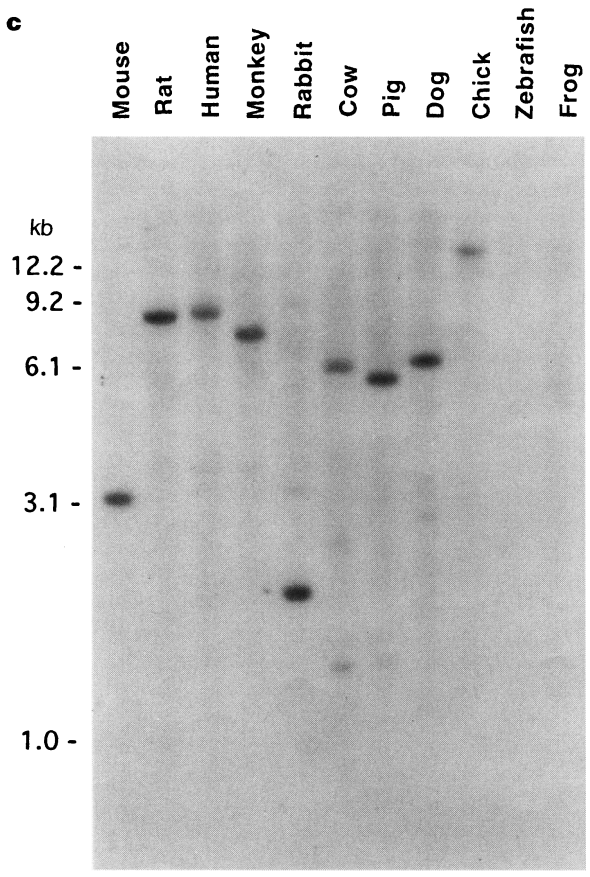

d

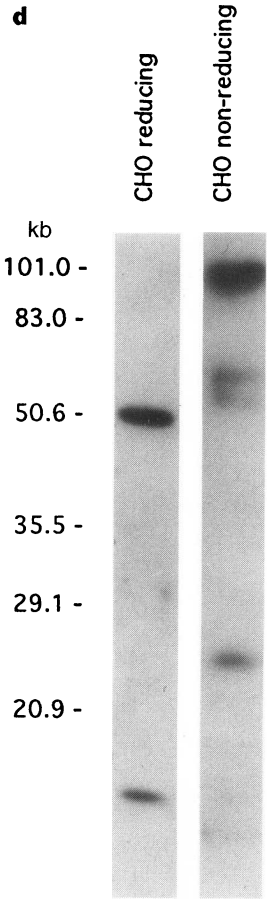

Figure 1 a, Amino-acid sequence of murine GDF-8. The predicted proteolytic processing site is underlined, and the conserved cysteine residues in the C-terminal region are marked by asterisks. The GenBank accession number for GDF-8 is U84005. **b**, Pairwise comparisons between mammalian TGF-β family members. Numbers represent per cent amino-acid identity beginning with the first conserved cysteine residue and extending to the C terminus. Subgroups of highly related sequences are boxed. Human sequences were used for all calculations except for nodal, GDF-3, GDF-7 and lefty, for which murine sequences were used. **c**, Genomic Southern analysis of DNA isolated from different species. **d**, Secretion, processing and dimerization of GDF-8.

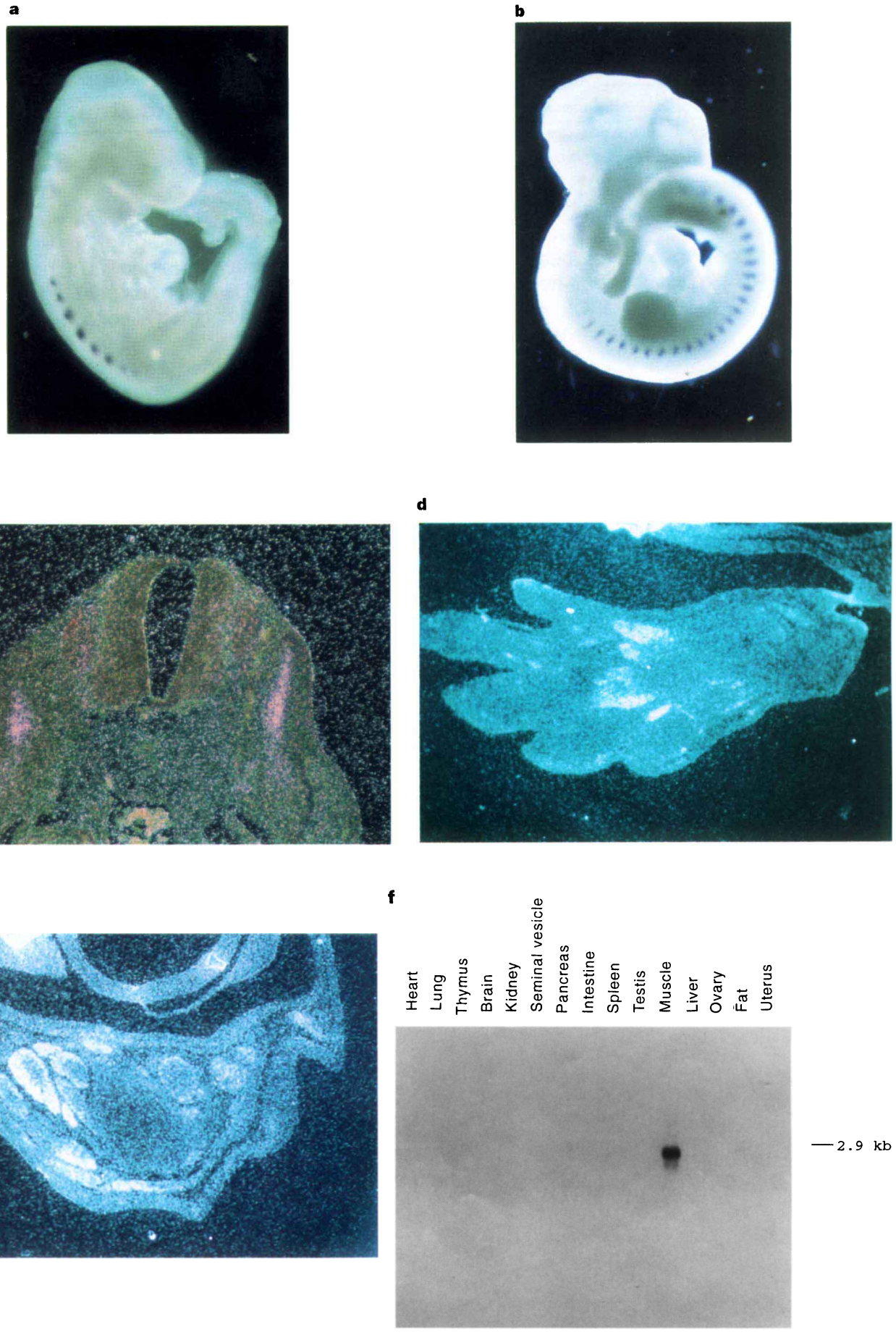
a
b
c
d
e
f
Heart
Lung
Thymus
Brain
Kidney
Seminal vesicle
Pancreas
Intestine
Spleen
Testis
Muscle
Liver
Ovary
Fat
Uterus
2.9 kb

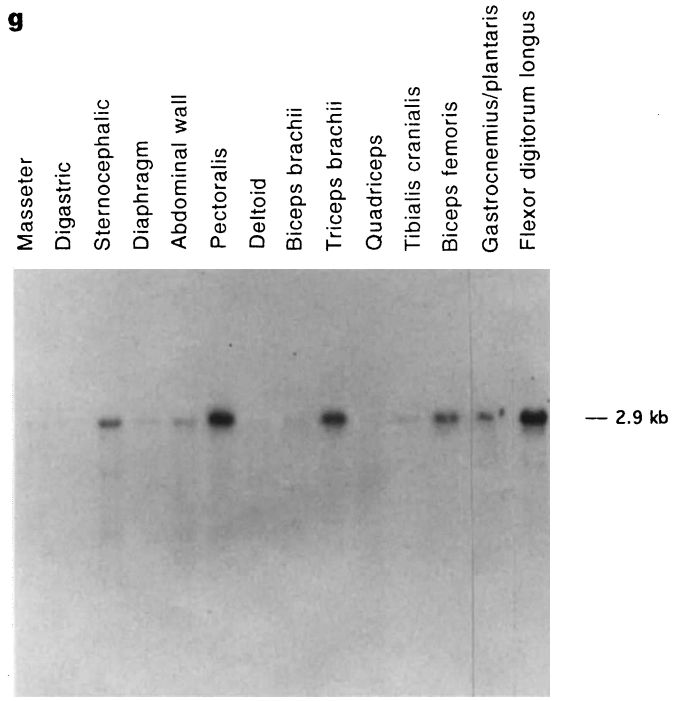

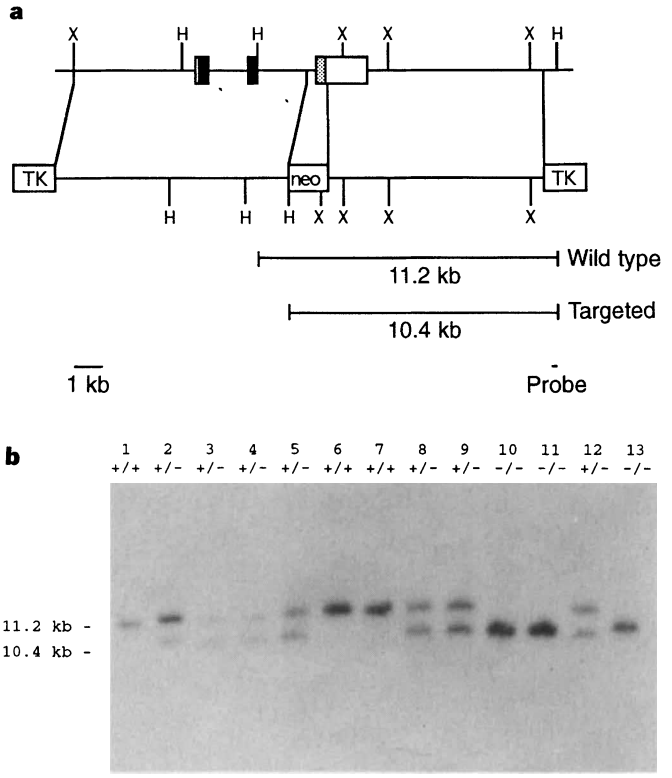

Figure 2 (Opposite and above) Expression of GDF-8 in murine embryonic and adult tissues. **a**, **b** Whole-mount *in situ* hybridization analysis of day 9.5 p.c. (**a**) and day 10.5 p.c. (**b**) mouse embryos. Hybridization is restricted to developing somites. **c**–**e**, *In situ* by hybridization analysis of sections prepared from paraffin-embedded embryos. **c**, Specific expression of GDF-8 in developing myotome in a horizontal section at the level of the forelimb of a day 10.5 p.c. embryo. **d**, **e**, Specific expression of GDF-8 in muscles of the developing foot and hip region, respectively, of day 14.5 p.c. embryos. No hybridization was seen using sense probes either on sections or for whole-mount analysis (data not shown). **f**, **g**, Northern analysis of adult tissues (5 μg of twice-poly(A)$^+$-selected RNA) and individual adult muscles (20 μg of total RNA).

Figure 3 Construction of GDF-8 null mice by homologous targeting. **a**, Map of the GDF-8 locus (top line) and targeting construct (second line). The black and stippled boxes represent coding sequences for the pro- and C-terminal regions, respectively. The white boxes represent 5′ and 3′ untranslated sequences. The targeting construct contains a total of 17 kb of homology with the GDF-8 gene. A probe derived from the region downstream of the 3′ homology fragment and upstream of the most distal *Hin*dIII site shown hybridizes to an 11.2 kb *Hin*dIII fragment in the GDF-8 gene and a 10.4 kb fragment in an homologously targeted gene. Abbreviations: H, *Hin*dIII. X, *Xba*I. **b**, Genomic Southern analysis of offspring derived from a mating of heterozygous mutant mice. DNA prepared from wild-type 129 SV/J mice (lane 1), targeted embryonic stem cells (lane 2), F1 heterozygous mice (lanes 3 and 4), and offspring derived from a mating of these mice (lanes 5–13).

($P < 0.001$).

Homozygous mutants were viable and fertile when crossed to C57BL/6 mice and to each other. Homozygous mutant animals, however, were about 30% larger than their heterozygous and wild-type littermates (Table 1). The difference between mutant and wild-type body weights appeared to be relatively constant irrespective of age and sex in adult animals. Adult mutants also displayed an abnormal body shape, with pronounced shoulders and hips. When the skin was removed from animals that had been killed, it was apparent that the muscles of the mutants were much larger than those of wild-type animals (Fig. 4a–d). The increase in skeletal muscle mass appeared to be widespread throughout the body. Individual muscles isolated from homozygous mutant animals weighed about 2–3 times more than those isolated from wild-type littermates (Table 2). Although the magnitude of the weight increase appeared to correlate roughly with the level of GDF-8 expression in the muscles examined (compare Table 2 with Fig. 2g), a more extensive quantification will be necessary to assess the significance of this trend.

To determine whether the increased muscle mass could account for the entire difference in total body weights between wild-type and mutant animals or whether many tissues were generally larger in the mutants, we compared the total body weights to carcass weights. As shown in Table 3, the difference in carcass weights between wild-type and mutant animals was comparable to the difference in total body weights. Moreover, because the fat content of mutant and wild-type animals was similar, these data are consistent with all of the total body weight difference resulting from an increase in skeletal muscle mass, although we have not formally ruled out the possibility that differences in bone mass might also contribute to the differences in total body mass.

To determine whether the increase in skeletal muscle mass resulted from hyperplasia or from hypertrophy, we carried out histological analysis of several different muscle groups. As shown in Fig. 4e, the mutant muscle appeared grossly normal. No excess connective tissue or fat was seen and there were no obvious signs of degeneration, such as widely varying fibre sizes (see below) or centrally placed nuclei. Quantification of the number of muscle fibres showed that at the widest portion of the tibialis cranialis muscle, the total cell number was 86% higher in mutant animals compared to wild-type littermates (mutant = 5,470 ± 121 ($n = 3$); wild-type = 2,936 ± 288 ($n = 3$); $P < 0.01$). Consistent with this result was the finding that the amount of DNA extracted from mutant muscle was roughly 50% higher than from wild-type muscle (mutant = 350 ± 69 μg ($n = 4$); wild-type = 233 ± 54 μg ($n = 3$) from pooled gastrocnemius, plantaris, triceps brachii, tibialis cranialis and pectoralis muscles; $P = 0.05$). Hence a large part of the increase in skeletal muscle mass resulted from muscle cell hyper-

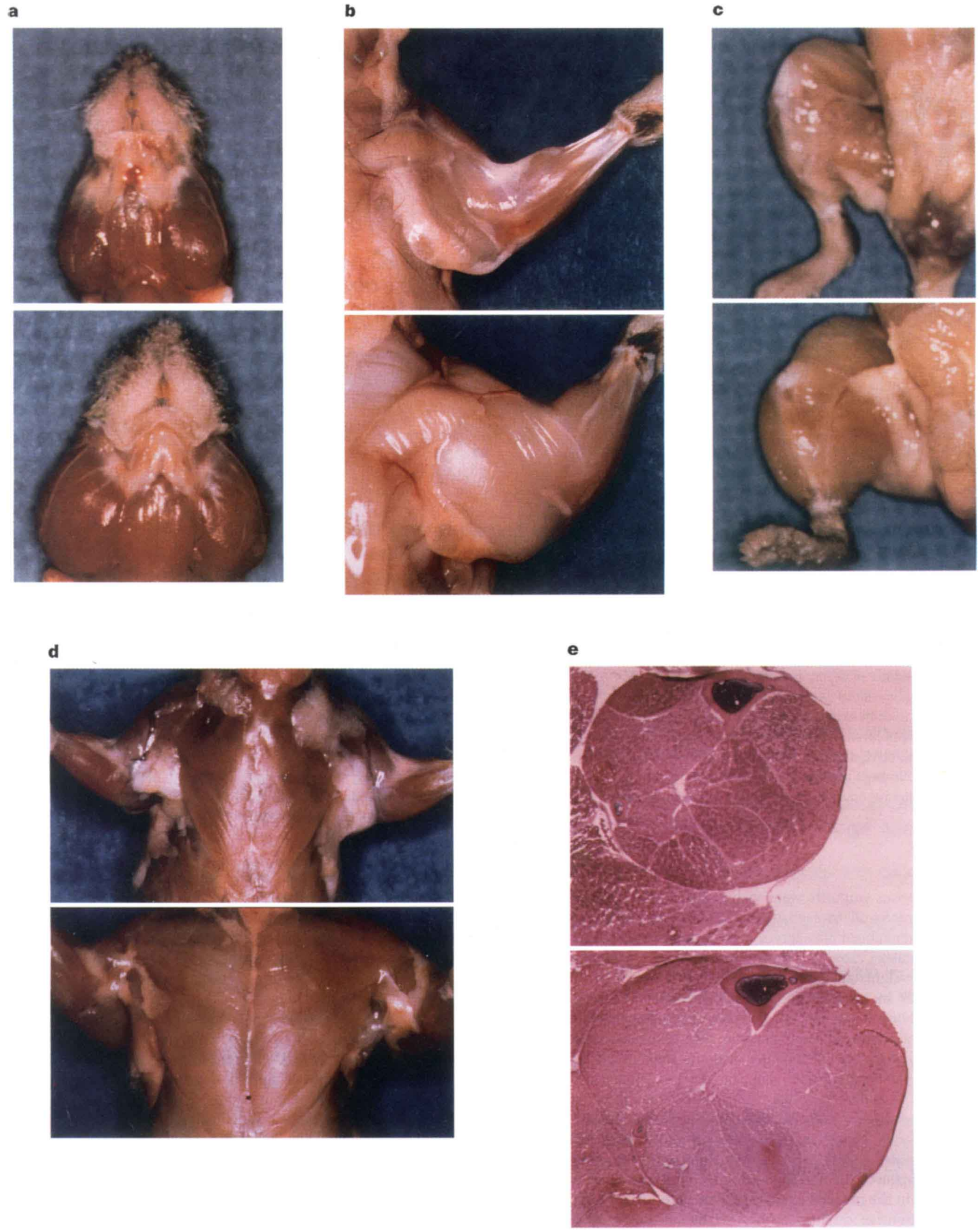

Figure 4 Increased skeletal muscle mass in GDF-8 null mice (bottom panels) compared to wild-type littermates (top panels). **a**-**d**, Facial (**a**), upper limb (**b**), lower limb (**c**) and pectoral (**d**) muscles of skinned animals. **e**, Sections of distal hindlimbs stained with haematoxylin and eosin.

plasia. However, muscle fibre hypertrophy also appeared to contribute to the overall increase in muscle mass. The mean fibre diameter of the tibialis cranialis muscle and gastrocnemius muscle was 7% and 22% larger, respectively, in mutant animals compared to wild-type littermates, suggesting that the cross-sectional area of the fibres was increased by about 14% and 49%, respectively. Notably, although the mean fibre diameter was larger in the mutants, the standard deviation in fibre sizes was similar between mutant and wild-type muscle (Fig. 5), consistent with the absence of muscle degeneration in mutant animals. The increase in fibre size was also consistent with the finding that the protein to DNA ratio (w/w) was slightly increased in mutant compared to wild-type muscle (mutant = 871 ± 111 ($n = 4$); wild-type = 624 ± 85 ($n = 3$); $P < 0.05$).

In several respects, the biological properties of GDF-8 resemble those of leptin[2,3]. Both GDF-8 and leptin are secreted molecules that are highly tissue-restricted in their expression patterns, and loss of GDF-8 or leptin function results in increased mass of the tissues that normally produce these factors. Leptin appears to exert its biological effect on adipose tissue indirectly by acting on the central nervous system. Additional experiments will be required to determine whether GDF-8 acts locally or systemically to regulate muscle mass and whether GDF-8 acts directly or indirectly on muscle cells. Elucidating the mechanism of action of GDF-8 will be important for understanding not only the role that GDF-8 plays in regulating muscle development but also the role, if any, that GDF-8 plays in processes such as development of rhabdomyoscarcomas, exercise-induced hypertrophy or regeneration following muscle injury. Ultimately, GDF-8 itself or molecules that inhibit GDF-8 signalling may prove useful in the treatment of musculodegenerative states such as muscular dystrophy, neuromuscular diseases, or cancer cachexia. Inhibiting GDF-8 function could also have important applications in agriculture; indeed, as we have shown, GDF-8 homologous sequences appear to be present in various farm animals, including chickens, cows and pigs.

Whatever the precise biological activity of GDF-8 may be, GDF-8 is unique among growth factor-like molecules in that loss of GDF-8 function leads to a dramatic and widespread increase in skeletal muscle mass. On the basis of the phenotype of GDF-8 null mice and the tissue-specificity of GDF-8 expression, we will hereafter refer to GDF-8 as myostatin. □

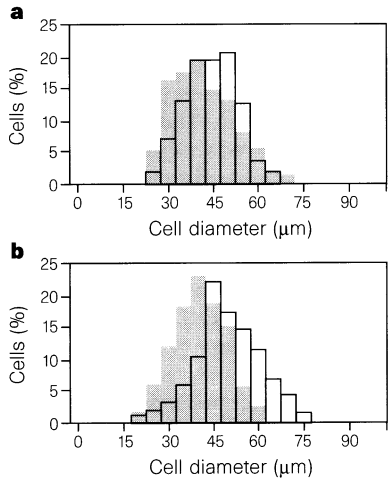

Figure 5 Muscle fibre size distribution in mutant (open bars) and wild-type (shaded bars) animals. Smallest cross-sectional fibre widths were measured for **a**, wild-type (n = 1,761) and mutant (n = 1,052) tibialis cranialis or **b**, wild-type (n = 900) and mutant (n = 900) gastrocnemius muscles, and fibre sizes were plotted as a per cent of total fibre number. Standard deviations were 9 and 10 μm, respectively, for wild-type and mutant tibialis cranialis and 11 and 9 μm, respectively, for wild-type and mutant gastrocneumius muscles.

Methods

Cloning of GDF-8. GDF-8 was identified from a mixture of PCR products obtained with primers SJL141 (5′-CCGGAATTCGGITGG(G/C/A)A(G/A/T/C)(A/G)A(T/C)TGG(A/G)TI(A/G)TI(T/G)CICC-3′), which encodes the amino-acid sequence GW(H/Q/N/K/D/E)(D/N)W(V/I/M)(V/I/M)(A/S)P, and SJL147 (5′-CCGGAATTC(G/A)CAI(G/C)C(G/A)CA(G/A)CT(G/A/T/C)TCIACI(G/A)(T/C)CAT-3′), the reverse complement of which encodes the amino-acid sequence M(V/I/M/T/A)V(D/E)SC(G/A)C. PCR using these primers was carried out with 2 μg murine genomic DNA at 94 °C for 1 min, 50 °C for 2 min, and 72 °C for 2 min for 40 cycles. PCR products were digested with *Eco*RI, and products about 280 nucleotides long were gel-purified and subcloned into Bluescript (Stratagene, La Jolla, CA). GDF-8 represented 4 out of 110 subclones analysed. A full-length murine GDF-8 cDNA clone was isolated by screening a muscle library using the partial GDF-8 sequence as a probe. The muscle cDNA library was constructed in lambda ZAPII according to the instructions provided by Stratagene and screened without amplification. Library screening and analysis of cDNA clones were carried out as described previously[4]. For genomic Southern analysis of different species, 20 μg DNA were digested with *Eco*RI, electrophoresed, blotted and probed with a C-terminal fragment of GDF-8. All DNA samples were obtained from Clontech (Palo Alto, CA) except for the frog and zebrafish samples, which were kindly provided by D. Brown and M. Halpern, respectively. Filters were hybridized in 5 × SSPE (50 mM sodium phosphate, 5 mM EDTA, 900 mM NaCl), 10% dextran sulphate, 50% formamide, 1% SDS, 200 μg ml^{-1} salmon sperm DNA, and 1% each of ficoll, bovine serum albumin and polyvinylpyrrolidone and washed in 2 × SSC, 1% SDS at 33 °C.

Protein analysis. The GDF-8 coding sequence was cloned into the pMSXND expression vector[5] and transfected into CHO cells. Following G418 selection, the cells were selected in 0.2 μM methotrexate, and conditioned medium from resistant cells was concentrated and electrophoresed on SDS gels. Conditioned medium was prepared by Cell Trends (Middletown, MD). For preparation of anti-GDF-8 serum, the C-terminal region of GDF-8 (amino acids 268 to 376) was expressed in bacteria using the RSET vector (Invitrogen, San Diego, CA), purified using a nickel chelate column, and injected into rabbits. All immunizations were carried out by Spring Valley Labs (Woodbine, MD). Western analysis using [^{125}I]iodoprotein A was carried out as described[6].

***In situ* hybridization and northern analysis.** For all *in situ* hybridization experiments, probes corresponding to the C-terminal region of GDF-8 were excluded in order to avoid possible crossreactivity with other members of the superfamily. Whole-mount *in situ* hybridization analysis was carried out as described[7] except that blocking and antibody incubation steps were carried out as in ref. 8. Alkaline phosphatase reactions were carried out for 3 h for day 10.5 embryos and overnight for day 9.5 embryos. Hybridization was carried out using digoxigenin-labelled probes spanning nucleotides 8–811 and 1,298–2,676, which correspond to the pro- region and 3′ untranslated regions, respectively. *In situ* hybridization to sections was carried out as described[9] using ^{35}S-labelled probes ranging from about 100–650 bases in length and spanning nucleotides 8–793 and 1,566–2,595. Following hybridization and washing, slides were dipped in NTB-3 photographic emulsion, exposed for 16–19 days, developed and stained with either haematoxylin and eosin or toluidine blue. RNA isolation, poly(A)$^+$ selection, and northern analysis were carried out as described previously[4].

Construction and analysis of GDF-8 null mice. A murine 129 SV/J genomic library was prepared in lambda FIX II according to the instructions provided by Stratagene. The structure of the GDF-8 gene was deduced from restriction mapping and partial sequencing of phase clones isolated from this library. Vectors for preparing the targeting construct were kindly provided by P. Soriano and K. Thomas. R1 ES cells (kindly provided by A. Nagy, R. Nagy and W. Abramow-Newerly) were transfected with the targeting construct, selected with gancyclovir (2 μM) and G418 (250 μg ml^{-1}), and analysed by Southern analysis. Homologously targeted clones were injected into C57BL/6 blastocysts and transferred into pseudopregnant females. Germ-line transmission of the targeted allele was obtained in a total of 9 male chimaeras from 5 independently-derived ES clones. Genomic Southern blots were hybridized at 42 °C as described above and washed in 0.2 × SSC, 0.1% SDS at 42 °C.

For whole-leg analysis, legs of 14-week-old male mice were skinned and treated with 0.2 M EDTA in PBS at 4 °C for 4 weeks followed by 0.5 M sucrose in PBS at 4 °C. For fibre number and size analysis, samples were directly mounted

and frozen in isopentane as described[10]. Sections (10–30 μm) were prepared using a cryostat and stained with haematoxylin and eosin. Muscle fibre numbers were determined from sections taken from the widest part of the tibialis cranialis muscle. Muscle fibre sizes were measured from photographs of sections of tibialis cranialis and gastrocnemius muscles.

Carcasses were prepared from shaved 4-month-old mice by removing all of the internal organs and associated fat and connective tissue. Fat content of carcasses was determined as described[11]. For protein and DNA analysis, muscles from 11–14-week-old males were dissected free of attachments, weighed and homogenized in 150 mM NaCl, 100 mM EDTA. Protein concentrations were determined using the Biorad protein assay. DNA was isolated by adding SDS to 1%, treating with 1 mg ml^{-1} proteinase K overnight at 55 °C, extracting 3 times with phenol and twice with chloroform, and precipitating with ammonium acetate and EtOH. The samples were then digested with 40 μg ml^{-1} RNase for 1 h at 37 °C, and following proteinase K digestion and phenol and chloroform extractions, the DNA was precipitated twice with ammonium acetate and EtOH.

Received 13 November 1996; accepted 11 February 1997.

1. McPherron, A. C. & Lee, S.-J. in *Growth Factors and Cytokines in Health and Disease* Vol. 1B (eds LeRoith, D. & Bondy, C.) 357–393 (JAI, Greenwich, 1996).
2. Friedman, J. M. & Leibel, R. L. Tackling a weighty problem. *Cell* **69,** 217–220 (1992).
3. Spiegelman, B. M. & Flier, J. S. Adipogenesis and obesity: rounding out the big picture. *Cell* **87,** 377–389 (1996).
4. McPherron, A. C. & Lee, S.-J. GDF-3 and GDF-9: two new members of the transforming growth factor-β superfamily containing a novel pattern of cysteines. *J. Biol. Chem.* **268,** 3444–3449 (1993).
5. Lee, S.-J. & Nathans, D. Proliferin secreted by cultured cells binds to mannose-6-phosphate receptors. *J. Biol. Chem.* **263,** 3521–3527 (1988).
6. Burnette, W. N. Western blotting: electrophoretic transfer of proteins from sodium dodecyl sulfate-polyacrylamide gels to unmodified nitrocellulose and radiographic detection with antibody and radioiodinated protein A. *Anal. Biochem.* **112,** 195–203 (1981).
7. Wilkinson, D. G. in *In situ Hybridization: A Practical Approach* (ed. Wilkinson, D. G.) 75–83 (IRL, Oxford, 1992).
8. Knecht, A. K., Good, P. J., Dawid, I. B. & Harland, R. M. Dorsal-ventral patterning and differentiation of noggin-induced neural tissue in the absence of mesoderm. *Development* **121,** 1927–1935 (1995).
9. Wilkinson, D. G., Bailes, J. A. & McMahon, A. P. Expression of the proto-oncogene int-1 is restricted to specific neural cells in the developing mouse embryo. *Cell* **50,** 79–88 (1987).
10. Brumback, R. A. & Leech, R. W. *Color Atlas of Muscle Histochemistry* (PSG, Littleton, MA, 1984).
11. Leshner, A. I., Litwin, V. A. & Squibb, R. L. A simple method for carcass analysis. *Physiol. Behav.* **9,** 281–282 (1972).

Acknowledgements. We thank P. Dunlap and T. Bunton for assistance in maintenance and analysis of mice, Y. Litingtung for advice on growing ES cells, E. Hsiao for assistance with statistical analysis, D. Nathans for comments on the manuscript and T. Zimmers for suggesting the name myostatin. A.C.M. was supported by training grants from the NIH. This work was supported by research grants from the NIH (to A.M.L.) and the Edward Mallinckrodt Jr Foundation and MetaMorphix Inc. (to S.-J.L.). Under an agreement between MetaMorphix, Inc. and the Johns Hopkins University, A.C.M. and S.-J.L. are entitled to a share of sales royalty received by the University from MetaMorphix. The University, A.C.M. and S.-J.L. also own MetaMorphix stock, which is subject to certain restrictions under University policy. S.-J.L. is a consultant to MetaMorphix. The terms of this arrangement are being managed by the University in accordance with its conflict of interest policies.

Correspondence and requests for materials should be addressed to S.-J.L. (e-mail: sejin_lee@qmail.bs.jhu.edu).

Mice lacking mitochondrial uncoupling protein are cold-sensitive but not obese

Sven Enerbäck*†‡, Anders Jacobsson*†‡, Elizabeth M. Simpson*‡, Carmen Guerra*, Hitoshi Yamashita*†, Mary-Ellen Harper§ & Leslie P. Kozak*

* *The Jackson Laboratory, Bar Harbor, Maine 04609, USA*
§ *Department of Biochemistry, Faculty of Medicine, University of Ottawa, Ottawa, Ontario K1H 9M5, Canada*
‡ *These authors contributed equally to this work.*

The mitochondrial uncoupling protein (UCP) in the mitochondrial inner membrane of mammalian brown adipose tissue generates heat by uncoupling oxidative phosphorylation[1]. This process protects against cold[2] and regulates energy balance[3]. Manipulation of thermogenesis could be an effective strategy against obesity[4–9]. Here we determine the role of UCP in the regulation of body mass by targeted inactivation of the gene encoding it. We find that UCP-deficient mice consume less oxygen after treatment with a β3-adrenergic-receptor agonist and that they are sensitive to cold, indicating that their thermoregulation is defective. However, this deficiency caused neither hyperphagia nor obesity in mice fed on either a standard or a high-fat diet. We propose that the loss of UCP may be compensated by UCP2, a newly discovered homologue of UCP; this gene is ubiquitously expressed and is induced in the brown fat of UCP-deficient mice.

The *Ucp* gene was inactivated by homologous recombination in embryonic stem cells (ES) with a targeting vector that replaced a *BamHI/BglII* fragment carrying exon 2 and part of exon 3 with the *neo*^{r} gene, thereby deleting an essential membrane-spanning domain[10–12] (Fig. 1). One correctly targeted D3 ES cell clone produced a chimaera that transmitted the targeted allele (*Ucp*^{tm1}) to progeny. Homozygous and heterozygous mice were recovered in the proportions expected for a single gene mutation. Northern blot analysis demonstrated that −/− mice lack *Ucp* messenger RNA of the correct size (Fig. 2a). A faint signal from RNA products, both larger and smaller, can be detected on overexposed films; however, the absence of any UCP by immunoblot analysis indicates that this RNA does not contribute to any detectable immunoreactive protein (Fig. 2b). Mice with only one intact copy (+/−) of the gene produce *Ucp* mRNA at levels comparable to wild type (+/+) mice, as expected for an inducible gene required for thermoregulation. No differences were seen in the levels of transcripts for mitochondrial-localized cytochrome oxidase, the adipocyte-specific aP2 protein (Fig. 2a), cytoplasmic or mitochondrial glycerol-3-phosphate dehydrogenases, the β3 adrenergic receptor or leptin (data not shown).

The brown adipose tissue of UCP-deficient mice has enlarged lipid vacuoles (Fig. 3), but in all other respects it appears normal, including in the shape of its mitochondria (data not shown). The increased lipid deposition is to be expected in the absence of an uncoupling mechanism to dissipate the protonmotive force across the mitochondrial membrane[13].

Given the importance of UCP in the regulation of energy expenditure in rodents and the ability of β3-adrenergic agonists to stimulate this energy expenditure through their exclusive effects on brown and white adipose tissue[14], we studied oxygen consumption in resting UCP-deficient mice before and after injection of the β3-adrenergic agonist CL 316,243. We found no significant differences in resting oxygen consumption (that is, preinjection values) between wild-type (+/+), heterozygous (+/−) and UCP-deficient (−/−) mice at 28 °C (Fig. 4a). The oxygen consumption after treatment with CL 316,243 was significantly blunted in UCP-deficient mice, however, compared to wild-type and heterozygous controls. Whereas there was an approximate doubling of resting oxygen consumption in the latter two groups, which is normal for rodents[15], in UCP-deficient mice stimulation was only 34%. These results indicate an abnormal response to β3-adrenergic stimulation, like that found for *Ucp*-DTA mice (*Ucp*-diphtheria toxin A chain transgenic mice), when the same protocol and equipment were used[7].

The effects of UCP deficiency on thermoregulation were assessed by exposing 41 (−/−) mice (23 males and 18 females, ranging in age from 27 to 85 days) to cold (5 °C). The time required to lose 10 °C of body heat was used as a measure of sensitivity to cold. Thirty-five (−/−) mice (85%) were cold-sensitive and six (−/−) mice (15%) were resistant to cold, that is, they maintained body temperature after 24 h in the cold (Fig. 4b). Within the cold-sensitive group, the onset of temperature loss varied from 1.5 to 9.5 hours and was independent of sex or age. The ten heterozygous mice tested were all resistant to cold. These results show that brown-fat thermogenesis is important for protecting both young and

† Present addresses: University of Göteborg, Dept of Molecular Biology, Medicinareg 9C, S-41390 Göteborg, Sweden (S.E.); The Wenner-Gren Institute, Stockholm University, Dept of Metabolic Research, S-10691 Stockholm, Sweden (A.J.); Dept of Hygiene, National Defense Medical College, 3-2 Namiki, Tokorozawa, Saitama 359, Japan (H.Y.).